

A PULSE RADIOLYSIS DC CONDUCTIVITY DETECTION TECHNIQUE WITH NANOSECOND TIME RESOLUTION

B. VOJNOVIC, R. F. ANDERSON and B. D. MICHAEL
Cancer Research Campaign Gray Laboratory, Mount Vernon Hospital, Northwood, Middlesex
HA6 2RN, England

(Received 8 August 1985; in revised form 25 September 1985)

Abstract—This paper describes a pulse radiolysis DC conductivity method in which the spurious signals generated by the charge of the electron pulse are suppressed, allowing the conductivity kinetics to be observed even during the electron pulse, in a single record, with a time resolution of ~ 5 ns. A hybrid junction transmission line transformer is used in a balanced circuit such that its differential response rejects spurious signals but enhances the conductivity signal. The transformer also rejects the effects of intrinsic conductance so that the method can be applied to the study of aqueous systems. Although primarily designed for sub-microsecond use, the response of the transformer has also been extended to longer times by electronic means so that observations up to $100 \mu\text{s}$ can be made; a rapid settling of the baseline is also achieved. The technique uses a conductivity cell design which permits simultaneous observation of conductivity as well as optical changes of the sample after irradiation. Several examples of the application of the method to the study of high- and low-conductance liquids are presented. The sensitivity of the method is such that it can be used with doses per pulse of a few cGy, which in aqueous systems, corresponds to changes in concentration of $\sim 10^{-8}$ mol dm $^{-3}$. Reaction rates up to 5×10^7 s $^{-1}$, corresponding to $t_{1/2} = 14$ ns, have been measured with this technique.

1. INTRODUCTION

THE MEASUREMENT of the transient change in the conductivity of aqueous and nonaqueous solutions following irradiation by a short pulse of electrons has become an accepted technique in the study of radiation-induced chemical reactions.⁽¹⁻¹⁴⁾ A wide variety of detection methods has been developed and, with the exception of microwave absorption techniques,^(7,8) all the methods^(1-6,9-14) rely on the measurement of current changes through a cell containing two or more electrodes. The voltage applied to the cell can be DC or AC and many systems permit simultaneous optical absorption measurements. AC methods^(2,9) have limited time resolution but are generally more suitable for use with high intrinsic conductivity samples as polarization and electrolysis problems are absent. Faster changes can, however, be measured with DC methods^(5,10-14) since their time resolution is not limited by the frequency of the applied voltage.

The improvement in time resolution has been achieved principally by the adoption of balanced detection methods which seek to eliminate the interfering and overloading effects on the detection circuits of the electron pulse charge. This problem becomes worse with short electron pulses to the extent that, at nanosecond times, the magnitude of the peak electron current picked up by the cell electrodes may be a few hundred times larger than the current due to the change in conductivity. However, if suitable cell configurations are adopted, the electron pulse current, which is of constant polarity, can be separated from the conductivity current changes which are of opposing polarities at the cell

electrodes. The detection system's differential or balanced inputs can be provided by electronic amplifiers,⁽²⁾ by the use of wideband balanced-to-unbalanced transformers⁽¹²⁾ or, more recently,⁽¹³⁾ by storing the two sets of transients taken at opposing polarizing voltages and then using software subtraction and averaging techniques to enhance the conductivity signal. Conductivity changes down to 5-10 ns after the electron pulse can be observed using this last method, but it does require the acquisition of several hundred transients, principally due to the limited dynamic range of present day high-speed digitizers. The method described here achieves comparable time resolution but is essentially a real-time technique.

The simultaneous observation of optical absorptions in the irradiated sample is desirable and, for this reason, conductivity measurements are often performed in modified silica cells. When silica is irradiated there is evidence that conducting species with lifetimes of a few tens of nanoseconds are produced^(14,15) and it is not readily possible to separate these conductivity changes from those of the sample within the cell. It has been shown that for work on a timescale faster than 100 ns silica cells are not suitable,^(12,14) and it is necessary to use a cell with conducting faces. Both the system described here and that of Janata⁽¹³⁾ use such cells. However, it is possible to perform simultaneous optical absorption measurements with the cell described here.

All the sections in a detection system for nanosecond work must be considered carefully and the conductivity cell, the balanced detection system and the associated amplifier will now be described.

More complete constructional details can be found in Ref. (14).

2. THE CONDUCTIVITY CELL

The accelerator used in the present work was a Van de Graaff machine producing 4 MeV electrons at currents up to 5A and in pulse widths down to 1.5 ns.⁽¹⁶⁾ We are fortunate at the Gray Laboratory that the accelerator and beam-bending magnet room are separated from the experimental room by a 1.5 m thick concrete wall and this considerably reduces the level of interference from the accelerator reaching the detection circuits. The main source of interference is the electron pulse itself, but provided that the pulse current is returned to the beam line via a direct path, the resultant RF field in the room will be of negligible magnitude. The arrangement we employ is shown in Fig. 1. The cell, which is conducting, is connected electrically to, but decoupled mechanically from the beam line by a flexible woven wire mesh. This provides a low-inductance return path for the pulse charge to the (grounded) beamline but reduces the effects of any vibrations on the beam line which may disturb optical measurements. The electron beam enters the cell through a 0.2 mm brass foil behind a collimating aperture; all internal surfaces of the cell are platinum-plated, although considerably cheaper rhodium plating has recently been found to be just as effective. The conductivity electrodes are accurately aligned with respect to the collimator and to two 3×3 mm optical ports; they are self-supporting and are linked to two 50 Ω connectors at the rear of the cell. If such a symmetrical construction is employed, and if the electron pulse is accurately aligned with the cell, the electron pulse signals at the output connectors will be identical. The electric field distribution between the electrodes when a po-

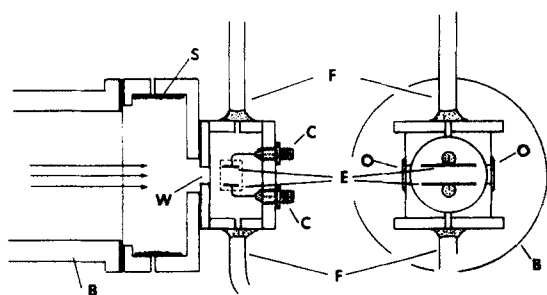


Fig. 1. The conductivity cell. Electrons emerging from the accelerator beam line B are collimated by aperture W which is accurately aligned with respect to the platinum cell electrodes E. The optical windows O are made out of suprasil silica and attached to the cell walls with epoxy. Flow pipes F are used for filling and emptying the internal circular cross-section cell volume. The electrodes E, 3×18 mm, are supported by SMB output connectors C. A wire mesh S is used to provide a low-inductance ground return path to the beam line for part of the electron pulse charge deposited in the collimator and cell walls.

larizing voltage is applied is, however, anything but parallel in a cell with conducting walls and therefore, the cell constant is difficult to predict. It should be stressed that the effective value of cell constant determined in the calibration of the system can only be obtained under similar experimental conditions to those in which the cell is used, and this is partly because of the inevitable nonuniformity of the electron dose distribution in the cell. AC bridge and standard KCl solution measurements are not suitable. The method used to determine the cell constant in the present case has been described previously⁽³⁾ and relies on the simultaneous observation of optical absorption at 350 nm and transient conductivity changes in a deaerated solution of tetranitromethane (10^{-3} mol dm $^{-3}$) and propan-2-ol (0.2 mol dm $^{-3}$) adjusted to pH 5 with perchloric acid.

3. BALANCED DETECTION SYSTEM

The electron pulse pick up can be largely eliminated and the conductivity signal enhanced by connecting the cell electrodes to a balanced input circuit where the like electron pulse pickup signals are subtracted and the unlike conductivity currents are summed. As has already been described,⁽¹²⁾ this can be conveniently performed by using a balanced transformer which has the additional advantage that

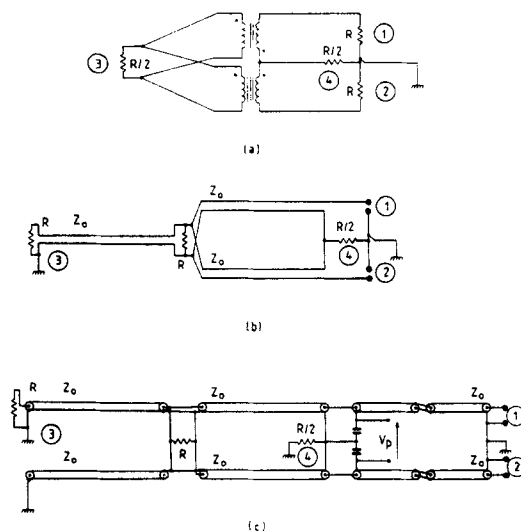


Fig. 2. The hybrid junction transmission-line transformer. The basic circuit, using conventional transformers, is shown in (a) where ports ① and ② are input ports, port ④ is the output sum port and port ③ the output difference (signal output) port. Transformers using transmission lines Z_0 replace the conventional transformers in (b) and in the final circuit (c), the polarizing voltage can be added at V_p . A compensation line (bottom left) is also added (note that the linear connection is not used) and the junction symmetry improved by balancing the leakage reactances at the junction. In (b) and (c) the transmission lines are loaded with ferrite cores which have been omitted from the drawing for the sake of clarity.

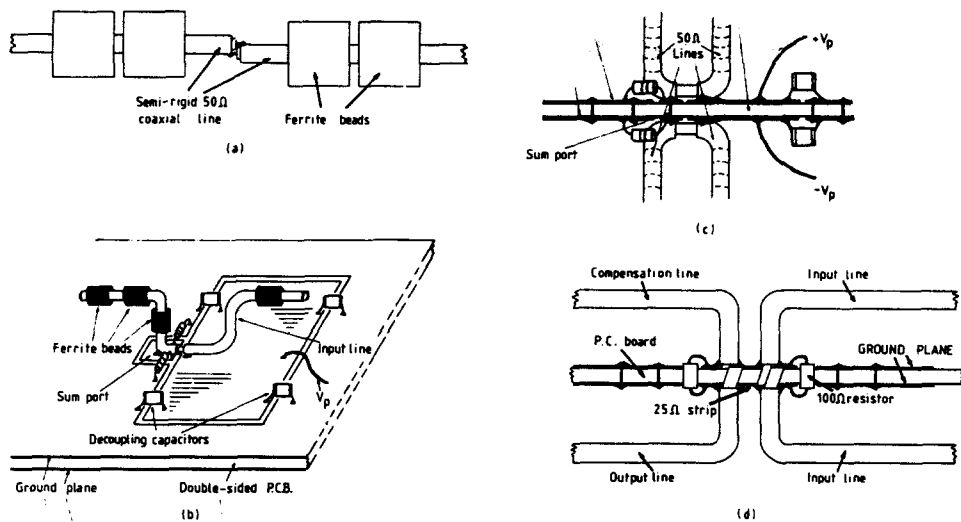


Fig. 3. Construction of the hybrid junction transmission-line transformer. (a) input section DC isolation junction; (b), (c) the sum port and decoupling arrangement; (d) the line junction and resistive pad, made up from $\frac{1}{4}$ W carbon resistors.

the intrinsic solution conductance signal can also be eliminated since the d.c. signal component is not transmitted by the transformer.

For wideband operation it is essential to use transmission-line transformers^(12,17,18) as described above. When these are wound in a balanced configuration, a limitation on the maximum common-mode signal which can be rejected is the poor isolation between the transformer inputs. The effect of this is that the ability of the transformer to reject similar signals at the two inputs, the common-mode rejection ratio (CMRR), is a function of the source impedance of the two signals. In the case of a conductivity cell, the source impedances are nominally similar but poorly defined since the cell is not a 50Ω source and problems arise due to multiple input-input reflections at times shorter than the signal transit time through the transformer.

In this work, a hybrid junction transmission-line transformer is employed,^(17,19-21) where the junction has been made symmetrical with a compensation line⁽²²⁾ and is preceded by two inverting transmission-line transformers⁽²³⁾ to enable injection of the cell polarizing voltage. The development of the hybrid junction using reciprocal two-port networks can be seen in Fig. 2. The principal property of the hybrid, that of coupling a signal from any one port to only two adjacent ports is exploited in the present design to achieve a high degree of input-input (port 1 to port 2) isolation. Both the sum and the difference of the two input signals are available at ports 3 and 4, but in the present design only the difference signal, corresponding to the conductivity signal is used. The sum signal, corresponding to the electron pulse charge intercepted in the cell, could be used in future versions for dosimetry purposes. This type of hybrid has equal conjugate impedances, but in this application it has been found con-

venient to pad the junction with 50Ω and use a 50Ω output line instead of a 25Ω line which is not readily available. Although this halves the output signal, the sensitivity of conductivity detection methods is considerably greater than that of optical methods and this loss is of little consequence.

Semirigid coaxial cable (0.056 in., type MA50056†), loaded with high-permeability ferrite ($\mu_r \sim 3000$, type FX4006, 4007 and 4016, 4017‡) was used in the construction of the hybrid and the inverting transformers. The lines are supported on a printed circuit board which serves as ground plane and as a microstrip structure for the junction (Fig. 3). Pulse and step responses of the hybrid are shown in Fig. 4, where the excellent CMRR (>300:1) and the good input isolation can be seen. The principal drawback of the structure is its relatively poor low-frequency response as the L/R decay time is 4.5 μs (where L is equivalent hybrid inductance, $R =$ hybrid equivalent load resistance). When used with amplifiers of 50Ω input impedance, it is only suitable for the observation of fast transients on a time-scale $\ll 1$ μs. However, since the decay-time constant is inversely proportional to loading resistance, it can be considerably improved if the device is operated into the input of a virtual-earth amplifier. A well-behaved high-frequency response requires the use of a 50Ω load, and it will be shown in the next section how to implement an amplifier with a frequency-dependent input impedance, namely 50Ω at high frequencies (>10 MHz) progressively reducing towards zero at lower frequencies where the L/R improvement is required. Ultimately, the decay time constant becomes limited by the cable resistance, so feedback techniques can be applied to

† Precision Tube Co. Inc., North Wales, PA, U.S.A.

‡ Mullard Ltd., London, U.K.

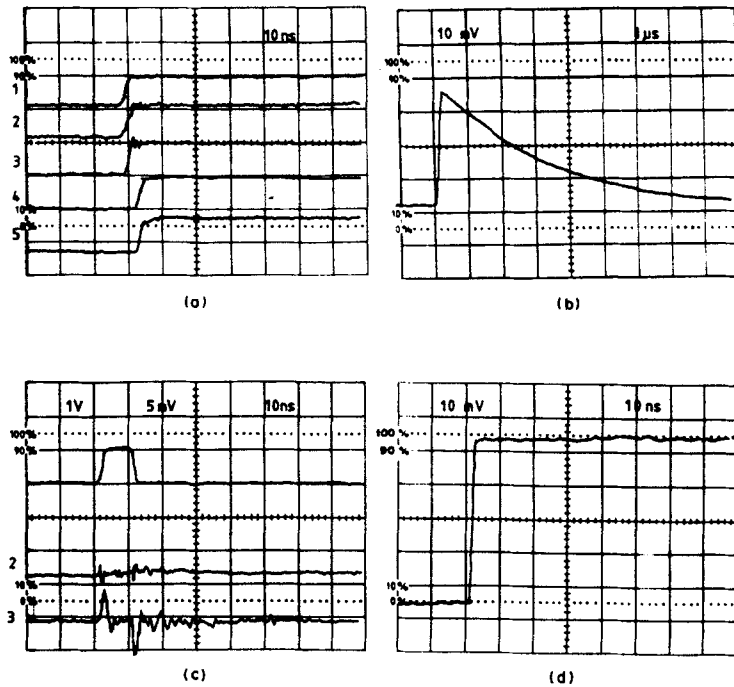


Fig. 4. Pulse and step responses of the hybrid junction transmission-line transformer. (a) Difference mode response: 1 input current step; 2 voltage at the driven input with the conjugate input terminated; 3 voltage at the driven input with the conjugate input open-circuited; 4 output voltage with conjugate input terminated; 5 output voltage with conjugate input open-circuited. These oscillograms depict desirable isolation between inputs of the device. (b) Difference mode low-frequency response; L/R time constant = $4.5 \mu\text{s}$. (c) Common-mode output response^(2,3) when the input is driven with a 10 ns wide pulse, 1; 2 shows the optimum balance (CMRR 300:1) while 3 shows an imbalance created by slight differences in the length of input leads ($\Delta l \approx 2 \text{ mm}$). (d) High-frequency difference mode response, 50Ω source and load impedance.

cause the amplifier input impedance to become negative, and thereby extend the decay time further.

The construction of the transformer can be seen in Fig. 5; the transformer is connected to the cell with two 12 cm lengths of RG179 cable and connected to the signal amplifier (Sec. 4) with a 15 cm length of RG179 cable. The signal amplifier is mounted on the transformer housing and its output

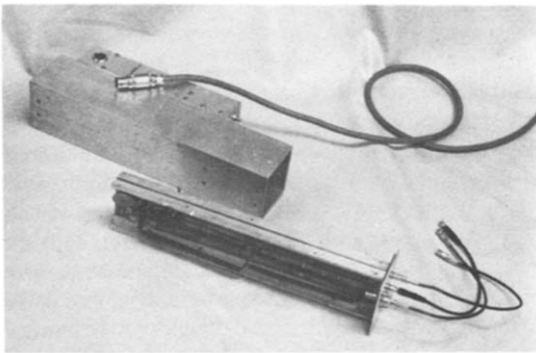


Fig. 5. The assembled transmission line transformer with the virtual-earth amplifier on the side of the housing ($5 \times 5 \times 25 \text{ cm}$). A screened multicore cable carries the polarization and amplifier power supplies and the trigger signal. This assembly is used close to the cell and the amplified signal taken out of the radiation area.

signal is taken out of the radiation area via 10 m of low-loss, a semirigid coaxial cable (Andrews FHJ4-50B†).

4. THE SIGNAL AMPLIFIER

The significant improvement in the low-frequency performance of the transformer is possible when it is realised that the transformer does not need to operate into a load that is matched at all frequencies. If the operation is visualized in terms of a response to a step function traveling along the transformer output line to a load, clearly only the rising edge of the step must be absorbed in the load. At times after the arrival of the step, the need for a correctly matched load becomes progressively smaller, so that at times much larger than the combined transit time of the line and transformer, matching is not required at all since the phase delay along the line is negligibly small.

In practice, a "correct" match is required for the first 50 ns or so after the arrival of the transient. A method of achieving such a frequency-sensitive transformer termination is shown in Fig. 6. It is as-

† Andrews Antenna Systems, Lochelly, Fife, Scotland.

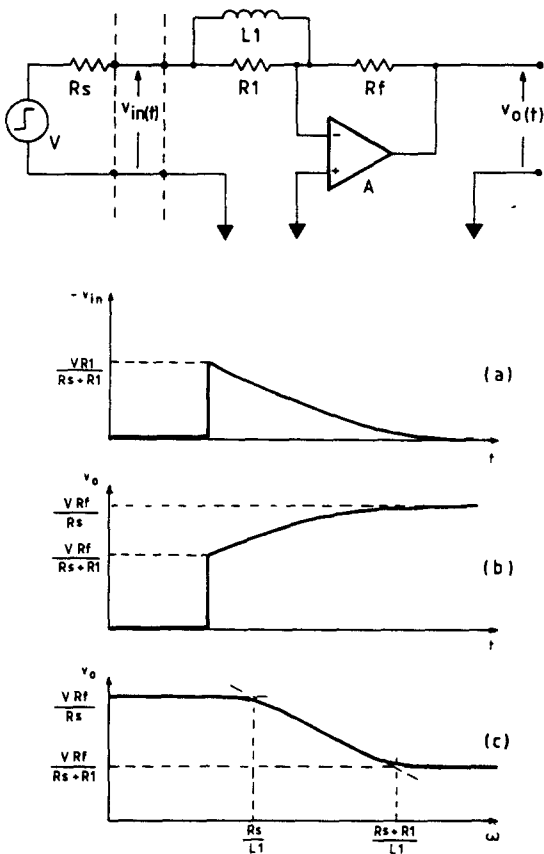


Fig. 6. A matched virtual-earth amplifier can be used to provide a frequency-sensitive termination for the hybrid junction transmission-line transformer, represented by V and R_s . The amplifier input and output responses to a transformer input step voltage are shown in (a) and (b) while (c) shows the overall frequency response.

sumed that a high-speed operational amplifier is used so that at high frequencies, where the reactance of L is large, the input impedance is determined by R_1 . At low frequencies, the input impedance is determined by the virtual-earth impedance $Z_v = R_f / (A + 1)$, where A is the open-loop gain of the operational amplifier. In the lower half of Fig. 6 trace (a) shows the variation of the input voltage $v_{in}(t)$ with time and is an indication of the corre-

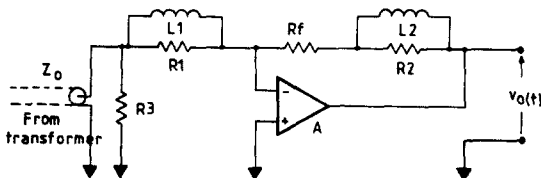


Fig. 7. A compensated matched virtual-earth amplifier is obtained by adding L_2 , R_2 in the op-amp's feedback path to lift the upper frequency response of Fig. 5(c). The output voltage $[V_o(t)]$ thus correctly reproduces an input step pulse.

sponding input impedance variation. At the output of the amplifier, a highly distorted version of the input step is obtained, as shown in trace (b), since the circuit frequency response exhibits two break points, trace (c).

It is nevertheless possible to straighten out the frequency and step responses of the circuit by introducing frequency-sensitive negative feedback. This can be done in a manner that complements the response of Fig. 6(c) and this is shown in Fig. 7. Components L_2 and R_2 are added in the feedback path such that a shelf-type of frequency response is obtained. Two conditions must be satisfied if correct compensation is to be achieved:

$$\frac{R_f}{L_2} = \frac{R_s'}{L_1}$$

and

$$\frac{R_f + R_2}{L_2} = \frac{R_s' + R_1}{L_1}$$

where R_s' is the resultant source impedance made up from the parallel combination of R_3 , the transformer source impedance, and the cell resistance. It is convenient in practice to make R_1 and R_3 equal so that, provided the cell resistance is high, R_s' is equal to 100Ω in parallel with the hybrid junction padding resistance, 50Ω , resulting in 33.3Ω .

This arrangement operates correctly only if the cell resistance is high compared to 33.3Ω , otherwise the frequency compensation will not be correct and the kinetics of the observed transients would be difficult to interpret. This restriction implies minimum cell resistances of 300Ω which corresponds to maximum solution conductances of $0.5 \times 10^{-3} \text{ S cm}^{-1}$ using the previously described cell. A similar limit is also reached with other DC conductivity methods because of the temperature rise of the solution during the time that the polarizing voltage is applied and because of the problems of gas formation at the electrodes.

Finally, the limiting effect on the low-frequency performance due to cable and connector resistances can be eliminated by making use of the noninverting terminal of the operational amplifier. The addition of positive feedback transforms the nominally zero virtual-earth impedance into a negative one. Any remaining cable and connector resistance can thus be eliminated by judiciously adding a controlled degree of positive feedback. Conversely, if signal inversion is introduced between the output and non-inverting input terminals of the operational amplifier, positive resistance is introduced in series with the virtual earth. This has the effect of decreasing the L/R time constant of the detection system.

It is therefore possible to control the decay-time constant of the detection system by changing the

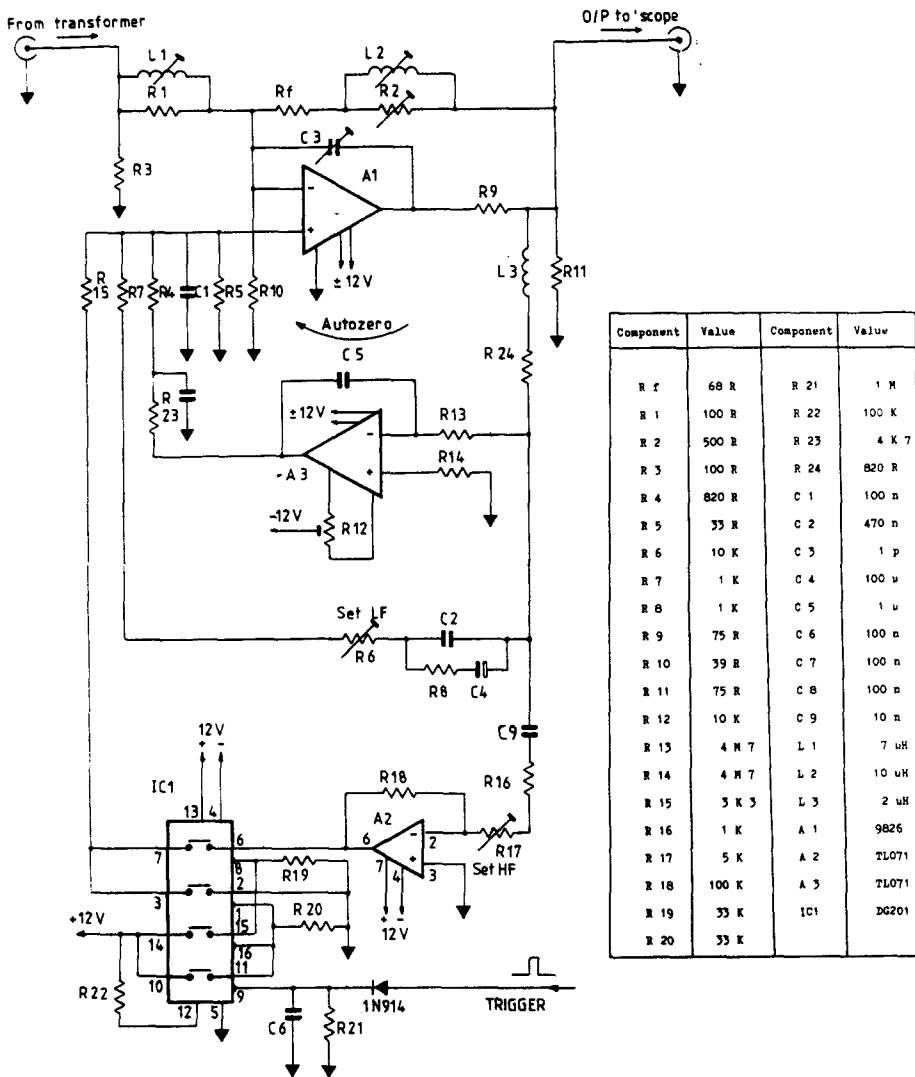


Fig. 8. The complete circuit diagram of the virtual-earth signal amplifier.

feedback at the noninverting input from negative to positive. If this changeover is done during the acquisition of the transient, a rapid settling of the conductivity signal after application of the polarizing voltage can be obtained followed by an extended decay time which allows the observation of slow reactions.

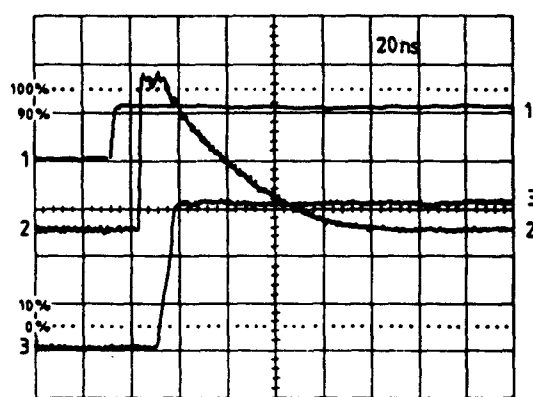
The complete signal amplifier circuit which incorporates these features is shown in Fig. 8. Operational amplifiers which are optimised for high-frequency use generally have a poor DC performance, so an integrating autozero loop with a time constant of 5 s, using amplifier A3, has been added. This arrangement maintains the quiescent DC level at A1 output at ground potential, within a few millivolts. The analogue switch IC1 maintains overall negative feedback around A1 through A2 and when triggered allows the positive feedback path R6, R7, R8, C2, C4 to become active. These components are used to shape the frequency response of the positive feedback loop so that it does not extend

down to DC. Resistor R6 is used to adjust the step response so that for the first 100 μs or so the L/R droop is negligible. Similarly, R17 is set for a low-frequency settling time of 1 μs before IC1 is triggered.

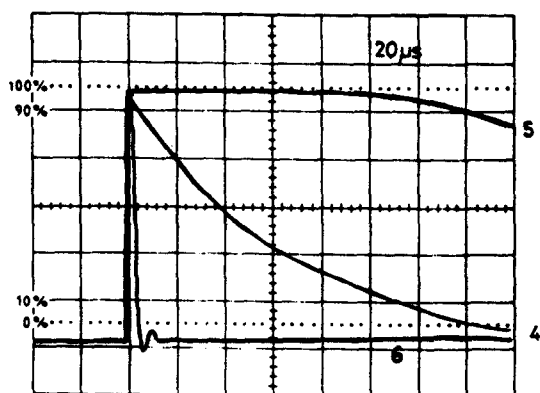
A1 must of course be an amplifier with a low-propagation delay and a high gain-bandwidth product. A device which has been found particularly useful is a type 9826† amplifier with a 1 GHz gain-bandwidth product, a 12 ns 0.1 percent settling time and a 3 ns delay time.‡ An output signal risetime of 6.3 ns is obtained with this arrangement; this is degraded to 6.7 ns when the hybrid junction transformer is added. In the present application it is more important to achieve a smooth step response with-

† Optical Electronic Industries, Tucson, AZ, U.S.A.

‡ More recently a type CLC104 amplifier from Com-linear Corporation, Loveland, CO, U.S.A. became available and <2 ns risetime should be possible with that device.



(a)



(b)

Fig. 9. Transient response of the virtual-earth amplifier. (a) 1 Transformer input current step. 2 Amplifier input voltage, showing how the input impedance reduces to zero in 100 ns (the ring at the start of the waveform is due to the presence of the oscilloscope probe). 3 Amplifier output voltage (150 mV peak). (b) Low-frequency performance improvement of the hybrid transformer when coupled with the virtual-earth amplifier. Trace 4 shows the improved L/R response when no positive feedback is employed (R_6 of Fig. 8 open-circuited). Trace 5: R_6 set to its optimum value where negligible droop is obtained for 100 μ s after which the output amplitude rapidly decays. Trace 6: settling time of amplifier when DG201 (Fig. 8) is triggered; this response is used when the polarizing voltage is applied and trace 5 response used during observation of transients.

out overshoots rather than the best risetime and several additional components are added to the basic circuit. Resistor R_9 isolates the amplifier output from any output circuit stray capacitance which would produce an unwanted additional pole in the open-loop response; the compensation capacitor C_3 is used to set the step response of the circuit. The closed-loop response of the 9826 is optimized for gains of $\times 3$ – $\times 5$ and resistor R_{10} is added to increase the noise gain of the circuit. It is essential

to employ high-frequency construction techniques in the implementation of the circuit; the performance is summarized in Fig. 9.

It should be pointed out that where the risetime of this amplifier is not adequate, the transformer can be used on its own or through a "conventional" amplifier of 50 Ω input impedance, with the limitation that the low-frequency decay time is limited to 4.5 μ s. We have found it convenient to use an amplifier made up from TO 5-cased microwave amplifier modules, GPD-461, GPD-462, GPD-463,[†] where a variable gain up to $\times 100$ with a bandwidth extending beyond 500 MHz is readily achieved. This 50 Ω amplifier can be used directly after the hybrid transformer for the fastest work, or can follow the virtual-earth amplifier if an enhanced detection sensitivity is required.

5. THE POLARIZATION VOLTAGE SUPPLY

The common-mode rejection of the hybrid transformer, although large, still dictates the use of high-polarizing voltages to maximise the conductivity signal in relation to the interfering effects of the electron beam. Ideally, a constant-power power supply would be used so that power dissipation within the cell is not exceeded, but a current-limited constant voltage supply is a simpler practical alternative. Rather than using a single supply at the V_p terminals of the hybrid transformer (Fig. 2), it has been found convenient to use two matched power supplies of opposite polarities connected between ground and each V_p terminal. In this way each isolation transformer is energized independently and a totally symmetric arrangement is obtained. In our case two supplies,[‡] variable 0–350 V and 0–200 mA, type PAB 350-0.1, are used so that up to 700 V can be produced across the cell. For aqueous work, however, only 100–300 V is commonly used, the higher voltages being primarily useful for studies on dielectric solvents⁽⁵⁾ where very high fields can be withstood.

The polarizing voltage is applied as a single pulse of 2–50 ms duration. Although the switching could be performed at the output of the power supplies, it has been found more convenient to modify the supplies so that logic level programming of these outputs is possible. More complex polarizing voltage waveforms have not been found useful.⁽¹⁴⁾ The slow risetime of the polarizing voltage (~ 2 ms) inherent in this approach is of little practical consequence. The actual output voltage is sampled 50 μ s before the radiation pulse for display on a $3\frac{1}{2}$ digit DVM.

[†] Avantek Corporation, Santa Clara, CA, U.S.A.

[‡] Kikusui Electronics Corp., Nakaharaku, Kawasaki, Japan.

6. CALCULATION OF CONDUCTANCE CHANGE

An equivalent circuit for the conductivity detection method described here is shown in Fig. 10. After the switch *S* is closed and the polarization current has settled to a steady value, the cell conductance can be considered to be made up of two components, the steady component G_c , and the transient component $G_c(t)$. These conductances give rise to two currents: $i_2(t)$ is the current which flows through the cell due to the intrinsic solution conductance, while $i_1(t)$ is the transient (additional) current which flows as a consequence of the radiation-induced change in the cell conductance. The inductance L is representative of the shunt inductance of the balanced transformer/hybrid. The effective load resistance $R'(t)$ can be either resistive (in the case of conventional amplifiers) or frequency, i.e. time dependent (in the case of the matched virtual-earth amplifier). Assuming that the polarizing voltage V_p is applied for a time before the electron pulse that is much greater than $L/R'(t)$:

$$(1) \quad V_p = R'(t)i_1(t) + \frac{i_1(t) + i_2}{G_c(t) + G_c}$$

hence

$$(2) \quad V_p G_c(t) = i_1(t)[1 + (G_c(t) + G_c)R'(t)] + \frac{R'(t)}{L} \int_0^t i_1(t) dt$$

The start of the electron pulse occurs at $t = 0$, that is when $i_1(t) = 0$. The magnitude of the final term in relation (2) is determined by the low-frequency time constant of the detection system. The time constant $L/R'(t)$ can usually be arranged to be much greater than the observation time t of the transient. Thus in general, the final term is negligible in comparison with the remainder and the relation can be simplified to

$$(3) \quad i_1(t) = \frac{V_p G_c(t)}{1 + R'(t)[G_c(t) + G_c]}$$

In addition, $G_c(t)$ is usually small compared with

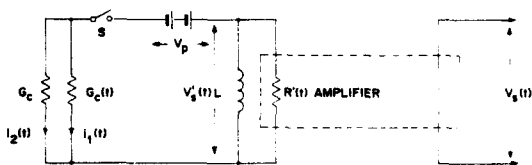


Fig. 10. Equivalent circuit of the conductivity detection system. A signal voltage $V_s'(t)$ is generated at the transformer output due to the transient conductance change $G_c(t)$. The amplified signal voltage $V_s(t)$ is measured by a 'scope or digitizer.

$[G_c + 1/R'(t)]$ and equation (3) can be simplified to

$$(4) \quad i_1(t) = \frac{V_p G_c(t)}{1 + R'(t)G_c}$$

It is therefore, clear that the output current is a linear function of the transient conductance charge. This output current causes a signal voltage $V_s(t)$ to appear at the input of the recording device (oscilloscope or digitizer). This voltage is related to the transient current by

$$(5) \quad V_s(t)T = i_1(t),$$

where T is the combined transconductance of the transformer and amplifier. Hence

$$(6) \quad V_s(t) = \frac{V_p G_c(t)}{T[1 + R'(t)G_c]}$$

Provided the intrinsic solution conductance G_c is small [compared with $1/R'(t)$], the above relation can be simplified to

$$(7) \quad V_s(t) = \frac{V_p G_c(t)}{T}$$

In the case of the virtual-earth amplifier, $R'(t)$ is negligible and this simplification is valid under all practical conditions. In the case of the 50Ω amplifier, the cell conductance must be determined independently and the correction applied [using eqn (6)] when dealing with cell resistances smaller than $10 R'(t)$. The load impedance of the transformer is reflected as the input impedance of the transformer [$R'(t)$] while any internal losses of the transformer are included in the effective value of T .

With reference to diagram (c) of Fig. 2, when the balun is connected to a 50Ω load, the input impedance at the hybrid junction is 25Ω (50Ω load in parallel with the 50Ω matching pad). This results in a reflected input impedance of $2 \times 50\Omega$, that is 100Ω balanced. The cell therefore, behaves as if connected to a current-measuring circuit of 100Ω internal impedance. A current injected at one of the balun inputs will be shared by the 50Ω load and by the 50Ω matching pad; hence, only half the signal voltage is available at the output. In the case of balanced conductivity signals, equal and opposite conductivity currents are present at the inputs, and these currents combine at the output. A conductivity current $i_1(t)$ thus results in a voltage $i_1(t) \times 50\Omega$. The transconductance of the transformer T is thus nominally $2 \times 10^{-2} \text{ AV}^{-1}$, giving $2 \times 10^{-3} \text{ AV}^{-1}$, and $2 \times 10^{-4} \text{ AV}^{-1}$ when followed by the 50Ω amplifier gains of $\times 10$ and $\times 100$, respectively. When connected to the virtual-earth amplifier, the feedback and input resistors determine the transconductance and result in a value of $8 \times 10^{-2} \text{ AV}^{-1}$.

TABLE 1. CONDUCTIVITY DETECTION CALIBRATION: MEASURED TRANSCONDUCTANCE VALUES T WHICH RELATE THE CONDUCTIVITY SIGNAL VOLTAGE OBTAINED AT THE OSCILLOSCOPE (DIGITIZER) INPUT TO THE CURRENT CHANGE IN THE CONDUCTIVITY CELL

Virtual-earth amp.	T/AV^{-1}		
	Direct connection	$\times 10$ 50 Ω amplifier	$\times 100$ 50 Ω amplifier
8.05×10^{-2}	2.16×10^{-2}	2.17×10^{-3}	2.17×10^{-4}

The measured values (Table 1) differ slightly due to losses in the lines and due to resistor tolerances.

The measured electrical changes are related to the changes in the cell, that is to the formation or neutralization of charges in the cell by the relation

$$\sigma(E) = KG_c(t) = C(t)[Z]\Lambda(C),$$

where $\sigma(E)$ is the solution conductivity change, K is the cell constant, $C(t)$ is the change in molar concentration of a particular species, Z is the electronic charge state of the species, and $\Lambda(C)$ is the equivalent conductivity of the species at concentration C .

The minimum detectable change in product of ion concentration and equivalent conductivity $\Delta[CA]_{\min}$ is therefore given by

$$\Delta[CA]_{\min} = \frac{K \times 10^3 \times \Delta v_{\min} \times T}{V_p} \text{ S cm}^2 \times \text{equiv}^{-1} \text{ mol dm}^{-3},$$

where Δv_{\min} is the minimum detectable signal voltage, V_p is the polarizing voltage and the cell constant is expressed in cm^{-1} . A typical V_p of 200 V is used; the value of Δ_{\min} is more difficult to estimate since it depends on whether successive transients are averaged and the precision to which the result is required. Assuming that only a single transient is acquired, referring to Fig. 11, an estimate of the signal amplitude (20 mV) to within $\pm 5\%$ can be made. This is equivalent to 200 μV at the input of the transformer. Assuming an equivalent conductivity for a $[\text{H}_{\text{aq}}^+ \text{-anion}]$ pair of 360 $\text{S cm}^2 \text{equiv}^{-1}$,⁽³⁾ transient concentration changes of such ion pairs of $7 \times 10^{-9} \text{ mol dm}^{-3}$ may therefore be detected in aqueous solution at nanosecond times. This typically corresponds to a pulse dose of less than 0.025 Gy. This detection limit is degraded by approximately eight times when the virtual-earth amplifier is used directly after the hybrid transformer [Fig. 11(c)].

The time resolution which can be obtained has been limited in our case by the available transient digitizer. A 7612D* digitizer has been used with a minimum slot width of 5 ns. Ultimately, the time resolution is determined by the risetime and the common-mode rejection ratio of the transformer. The perturbation in the detection electronics is

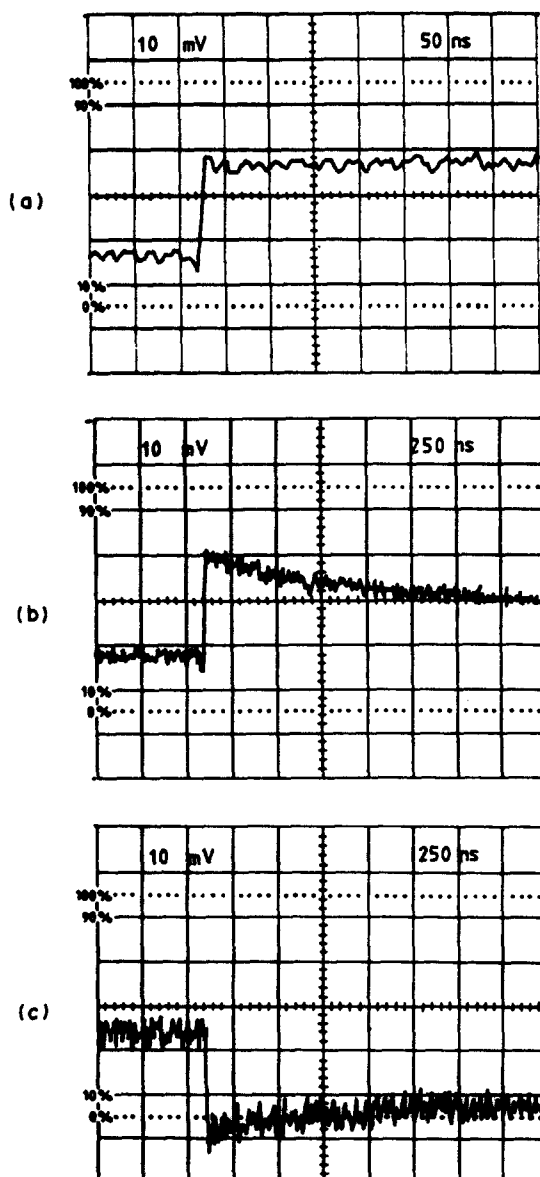


Fig. 11. The limiting noise performance of the conductivity detection system: deaerated water irradiated with 10 ns electron pulses, 3.5 MeV, 200 V polarization: (a) 50 Ω amplifier, gain $\times 100$, equivalent input sensitivity 0.1 mV div^{-1} , 2.2×10^{-6} A div^{-1} cell current, dose ≈ 0.025 Gy; (b) same conditions as in (a) but showing the L/R droop of transformer; (c) transformer operating into the virtual-earth amplifier followed by a $\times 100$ voltage amplifier, sensitivity 8 $\times 10^{-6}$ A div^{-1} cell current, dose ≈ 0.09 Gy.

* Tektronix, Inc., Beaverton, OR, U.S.A.

caused by the high-frequency components in the pulse spectrum while the magnitude of the conductivity signal determines how significant the perturbation will be. Practical results indicate that observations can be made approximately 5 ns after the beginning of a 1.5 ns electron pulse when an oscilloscope (Tektronix 7844, 7A19 plug in, 350 MHz bandwidth) and camera are used to record the transient (single shot). When the virtual-earth amplifier is used, this figure degrades to 9 ns after the beginning of a 1.5 ns electron pulse; this is due to amplifier risetime limitations. When the digitizer is employed, the time resolution is degraded further because of the digitizer's input bandwidth (90 MHz) and because the digitizer clock is not synchronized with the electron pulse; the net effect is that a minimum of two slot widths (10 ns) are required for a confident observation.

It should be stressed that the present methods, unlike any previously described technique, is capable of resolving the build up of the conductivity signal during a nanosecond electron pulse. Pulse

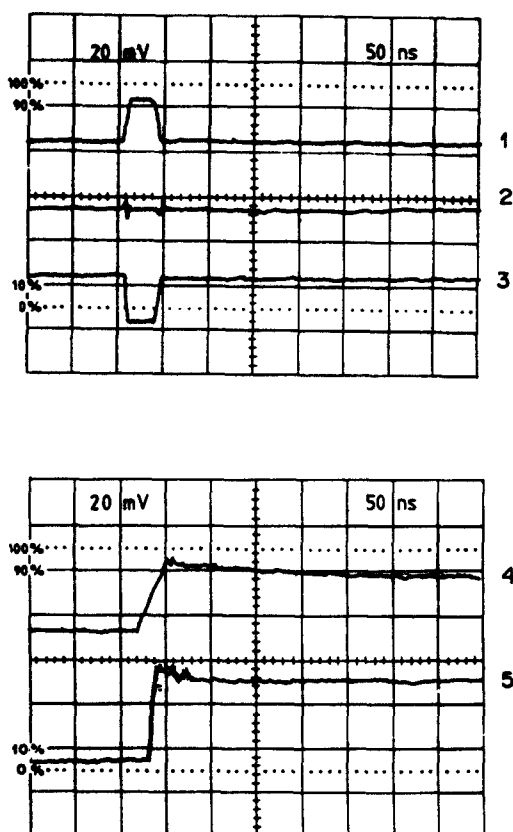


Fig. 12. Electron pulse interference rejection of the detection system. 1–3 cell filled with deaerated water, zero polarizing voltage, 30 ns electron pulse; 1 electron beam misaligned so that pick up is too large on top electrode; 2 optimal alignment of electron beam; 3 electron beam misaligned so that pick up is too large on bottom electrode; 4 correctly aligned beam, 200 V polarization, showing that the conductivity signal can be resolved during 30 ns electron pulse; 5 as in (d) but using a 10 ns electron pulse showing increased interference due to $3 \times$ larger peak electron current.

widths of 30, 10, 4, 1.5 ns are available from our accelerator; the build up can be readily observed when 30 and 10 ns pulses are used and just observed with 4 ns pulses.

It should also be pointed out that although this technique is essentially a single-shot one, two transients are typically acquired; they are taken with opposite polarizing voltage polarities and subtracted from each other. In this fashion, any remaining common-mode electron pulse interference is further reduced and electrode polarization or electron beam misalignment effects are largely eliminated.

7. RESULTS

In this section a number of results are presented that demonstrate the capabilities of the technique. The ability of the method to reject the electron pulse is shown in Fig. 12(a). The top and bottom traces are obtained when the electron beam is steered nearer to one or other of the cell electrodes while the centre trace represents the optimally balanced condition. In this latter case, the conductivity signal build up can be readily resolved as shown in Fig. 12(b). In Fig. 13, simultaneous optical and conductivity changes are measured in water at near neutral pH. In this case each transient is the average of two transients taken at opposite polarizing voltages as discussed above. Such measurements have been

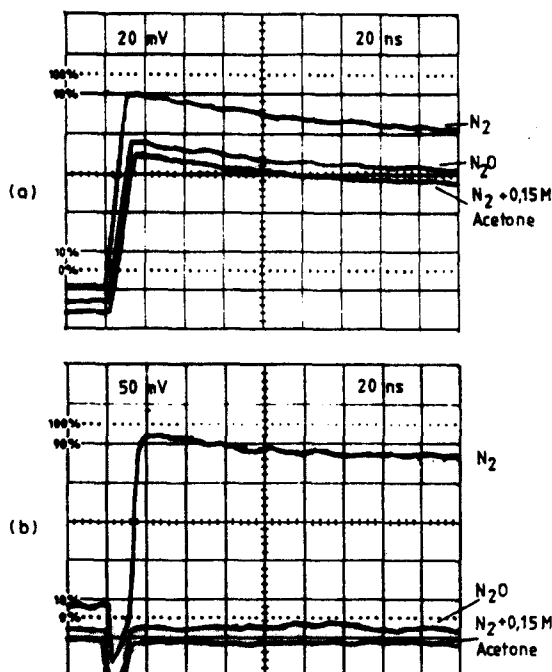


Fig. 13. Simultaneous observations of conductivity (a) and optical (b) changes in water at pH 6.3. In (b) the hydrated electron absorption ($\lambda = 600$ nm) is suppressed in N_2O -saturated water or in water with 0.15 M dissolved acetone. In (a) the conductivity traces show only partial attenuation in the presence of these electron scavengers.

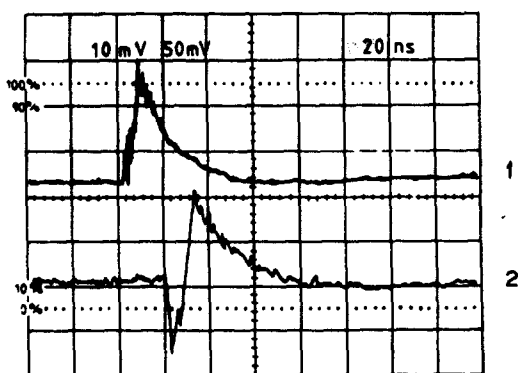


Fig. 14. Simultaneous observations of conductivity (1) and optical, ($\lambda = 700$ nm), (2) changes in deaerated water adjusted to pH 2.4 with perchloric acid. These single-shot transient pairs were recorded on Polaroid film, showing that the conductivity signal can be just resolved during a 4 ns wide electron pulse.

used to determine the yield of radiation-induced species⁽²⁴⁾ and to establish directly the yields of H_3O^+ and OH^- both inside the spur and those which escape the spur. Finally, Fig. 14 demonstrates the applicability of the technique to the study of high reaction rates. The cell contained water adjusted to pH 2.4 with perchloric acid and the figure shows that reaction rates exceeding $5 \times 10^7 \text{ s}^{-1}$ can be measured.

This detection system has also been used to study reaction kinetics in nonpolar solvents.⁽⁵⁾ The yields in that case are much smaller because of the low charge mobilities. On the other hand, high polarizing voltages can be used because the quiescent conductivity is negligible. The high dielectric breakdown strengths of such liquids enable the cell constant to be reduced (to 0.05 cm^{-1}) and the system has proved useful for studies of space-charge effects down to very low doses (<20 cGy).

CONCLUSION

DC conductivity methods provide a higher sensitivity than optical techniques for the detection of radiation-induced chemical changes. For aqueous work, the time resolution which could be achieved in practice has hitherto been limited by the interfering effects of the electron pulse charge deposited in the cell and could be improved only by averaging and subtracting a very large number of transients. The present technique uses a balanced arrangement where the effects of the electron pulse are largely eliminated so that the conductivity signal build up can even be resolved during a nanosecond radiation pulse. It has a time resolution of <5 ns and can provide results in a single shot, although typically a small number of transients is acquired.

Radiation-induced artefacts in the walls of the conductivity cell, which cause errors at times <100 ns, have been eliminated and the cell design permits

the simultaneous observation of optical and conductivity changes. A single detection system can cover the time range 10 ns–100 μs , with negligible baseline shifts even with intrinsic solution conductances of up to $0.5 \times 10^{-3} \text{ S cm}^{-1}$. It should be possible to extend the observation times if a higher inductance transformer is used, although in practice AC methods are more suited for work on these timescales because of the absence of electrode polarization and electrolysis problems.

Acknowledgements—The authors wish to express their thanks to D. S. Sehmi who developed the software necessary to interface the digitizer and process its data, to B. H. Bloomfield and C. T. Battey of the workshop of the Gray Laboratory for their help in the mechanical construction and to B. L. Hall, R. G. Newman, and K. D. Allen for their patience in providing the stable electron beams required for these experiments. Particular thanks are due to Dr E. M. Fielden and Dr R. L. Maughan for many helpful discussions during the development of the technique. The support of the Cancer Research Campaign is gratefully acknowledged.

REFERENCES

1. J. W. BOAG, G. E. ADAMS and E. J. HART, *Physical Processes in Radiation Biology* (Edited by L. Augenstein, R. Mason and B. Rosenberg), p. 247. Academic Press, New York, 1964.
2. K. H. SCHMIDT, *Int. J. Radiat. Phys. Chem.* 1972, 4, 439.
3. K.-D. ASMUS, *Int. J. Radiat. Phys. Chem.* 1972, 4, 417.
4. K. M. BANSAL and R. W. FESSENDEN, *J. Phys. Chem.* 1976, 80, 1743–1745.
5. M. P. DE HAAS, J. M. WARMAN and B. VOJNOVIC, *Radiat. Phys. Chem.* 1984, 23, 61–65.
6. G. BECK, *Rev. Sci. Instr.* 1979, 50, 1147–1150.
7. M. P. DE HAAS, *The Measurement of Electrical Conductance in Irradiated Dielectric Liquids with Nanosecond Time Resolution*. Delft University Press, Netherlands, 1977.
8. J. M. WARMAN, M. P. DE HAAS and J. B. VERBERNE, *J. Phys. Chem.* 1980, 84, 1240–1248.
9. J. LILIE and R. W. FESSENDEN, *J. Phys. Chem.* 1973, 77, 674–677.
10. T. E. ERIKSEN, *Chem. Scripta* 1975, 7, 193.
11. J. H. BAXENDALE, J. P. KEENE and E. J. RASBURN, *J. Chem. Soc. Faraday I* 1974, 70, 718.
12. R. L. MAUGHAN, B. D. MICHAEL and R. F. ANDERSON, *Radiat. Phys. Chem.* 1978, 11, 229–238.
13. E. JANATA, *Radiat. Phys. Chem.* 1982, 19, 17–21.
14. B. VOJNOVIC, Ph.D. thesis, University of London. The measurement of radiation-induced transient conductivity in aqueous solutions on a nanosecond time-scale, 1983.
15. R. C. HUGHES, *Phys. Rev. Lett.* 1973, 30, 1333–1336.
16. R. L. MAUGHAN, A. S. HALL, M. J. ROPER, B. D. MICHAEL and J. F. FOWLER, *Proc. Fourth Symp. Neutron Dosimetry*, Vol. II, pp. 5–15. EUR 7448, 1981.
17. C. L. RUTHROFF, *Proc. IRE* 1959, 47, 1337–1339.
18. R. E. MATICK, *Proc. IEEE* 1968, 56, 47–62.
19. IRE 1955, *Proc. IRE* 1955, 43, 1073–1074.
20. S. REHNMARK, *IEEE Trans.* 1977, MTT25 (10).
21. G. J. LAUGHLIN, *IEEE Trans.* 1976, MTT24 (3), 135–141.
22. R. BASSET, *Microwaves* 1980, 19(7), 47–52.
23. L. H. LUTHJENS and A. M. SCHMIDT, *Rev. Sci. Instrum.* 1973 44, 567–570.
24. R. F. ANDERSON, B. VOJNOVIC and B. D. MICHAEL, *Radiat. Phys. Chem.* 1985, 26, 301–303.